Virtual Admittance Based Switch Fault Detection for Hybrid UAVs

Taehyung Kim
Electrical and Computer Engineering
University of Michigan-Dearborn
Dearborn, MI, 48128 USA
taehyung@umich.edu

Sahithya Parvathareddy
Electrical and Computer Engineering
University of Michigan-Dearborn
Dearborn, MI, 48128 USA
sahip@umich.edu

2024 IEEE Energy Conversion Congress and Exposition (ECCE) | 979-8-3503-7606-7/24/$31.00 ©2024 IEEE | DOI: 10.1109/ECCE55643.2024.10861023

***Abstract*— Unmanned aerial vehicles (UAVs) are widely used for various applications, such as military surveillance and reconnaissance; delivery of packages; monitoring of plants and buildings; and search and rescue. Besides basic battery-electric propulsion, in order to improve range and endurance, hybrid electric propulsion systems based on combinations of batteries, fuel cells, solar cells, and ultracapacitors are increasingly being applied to these UAVs. For small- and medium-scale UAVs, the solar and fuel cell converters have non-isolated DC-DC converters that include a high-frequency switching device. In this paper, a novel switch fault detection technique based on virtual admittance is proposed for DC-DC converters. A fault index function is formulated based on the virtual admittance to minimize potential influence by highly dynamic load change while reducing computation complexity to implement the technique in cost-effective UAVs. The proposed technique has been verified by simulations and experiments to validate the feasibility of the approach.**

***Keywords*— UAV, switch fault, DC-DC converter**

I. Introduction

Electrically powered unmanned aerial vehicles (UAVs) and drones are widely used for various military and commercial missions, including mapping, inspection, surveillance, disinfection, delivery, and more. Electrical propulsion of these aircraft provides several notable advantages over internal combustion engines due to higher efficiencies at small size and lower vibration [1]–[3]. Hybridized power systems for these small-scale aircraft can offer further benefit, with longer endurances surpassing the range limitations of single-power-source unmanned aircraft [1]–[2].

These advanced hybrid electric UAVs and drones can be deployed for wider application areas, including emergency medical supply deliveries, rescue missions, and disinfection to sanitize facilities, especially for natural disasters and global pandemics. The demand for reliable long-range UAVs is increasing significantly due to the newer applications that require increased flight range. For a hybrid electric power system structure, redundancy is one of the easiest ways to enhance reliability. However, redundancy will increase system cost and weight, which can be a significant burden for small-scale aircraft.

For the power MOSFETS used in UAVs, switch faults occur mostly because of bond wire degradation, gate-oxide degradation, cracks and delamination in the die-attach solder, and connector failure [4].

The switch fault diagnosis for non-isolated dc-dc converters has been reported in the literature [5]-[16]. Among the existing switch fault diagnosis for non-isolated DC-DC converters, an auxiliary winding [5] and a Rogowski coil sensor [8] are used to extract fault indicators through the inductor voltage. The auxiliary-winding and coil-sensor based approaches require extra effort to install them in the existing inductors. The inductor current derivative [6], [7], [9], DC-link current derivative [10], and capacitor current derivative [11] are also used to diagnose converter switch failure. The methods with current derivatives are sensitive to signal noise due to the derivative procedure. Magnetic near-field waveforms along with a fast Fourier transform are utilized in [12] to detect switch faults. However, the cost of the magnetic probes to capture the waveforms and the computational burden for Fourier transformation are obstacles to use the method. In the proposed approach, extra coils or probes are not used due to the system cost. In addition, derivatives and fast Fourier transformation are also not considered. In this work, a method that can detect switch faults accurately with reasonable computational effort has been investigated. This approach focuses on a virtual admittance of the converter inductance at a switching frequency based on observations that both open-circuit fault and short-circuit fault do not create high-frequency inductor current ripple due to no switching operation occurring after the faults.

The proposed approach uses measured main inductor current and constructed inductor voltage based on the PWM signal, duty ratio, input dc voltage, and dc-link voltage. The current and voltage go through several steps with signal processing to extract a high-frequency component at the switching frequency. Then, α-β to d-q transformations are introduced to derive dc components to create a virtual admittance component that changes as a variable dc signal to compare it to a fault threshold to detect the fault. The virtual admittance configuration can provide a stable fault index formulation since a load change can influence both the inductor current component (numerator) and the inductor voltage component (denominator), which would eventually compensate for the influence. The proposed approach has been tested both by simulations and experiments. The feasibility of the fault detection method has been discussed to verify the proposed work.

This work was supported by the National Science Foundation grant, award no. 2321681.

II. Proposed Approach

For small- and medium-scale UAVs, the solar and fuel cell converters have non-isolated DC-DC converters [1]–[3] that include a high-frequency switching device and a diode, as shown in Fig. 1. If the S_F or S_{SO} switch (shown in Fig. 1 (b)) has a short fault, the current flowing through the switch increases rapidly, and hence the fast fuse (F_1 if S_F fails and F_{SO} if S_{SO} fails) will be activated and the switch leg will be open due to the high current. Therefore, the short fault will eventually result in an open circuit in this case.

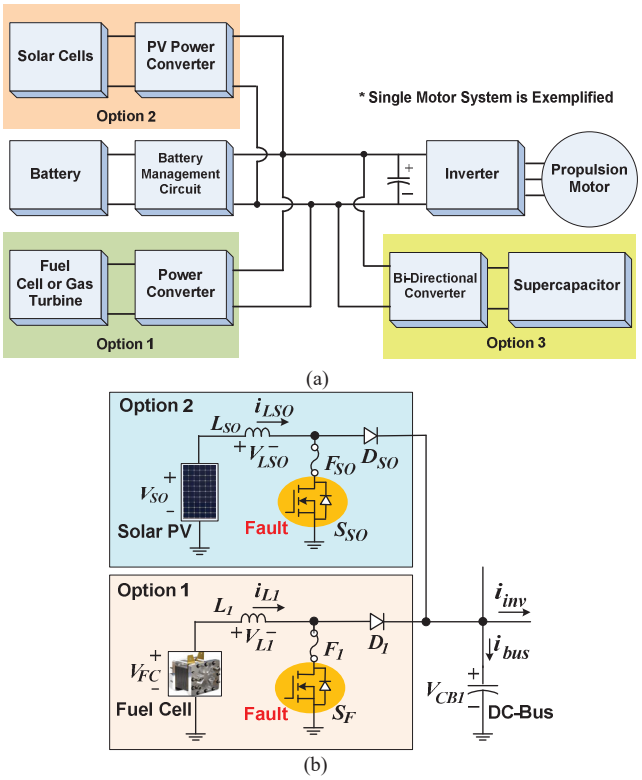

Fig. 1. (a) Hybrid configurations of long endurance hybrid electric UAVs with additional power source options, (b) Fuel cells and solar PV converters under a switch fault.

For both open switch fault (OSF) and short switch fault (SSF), the current flow toward the high-frequency switch will be disabled eventually. The hybrid electric UAVs can employ several DC-DC converters, as shown in Fig. 1(a), for the fuel cell, battery, solar cells, and ultracapacitor if all optional power sources are present.

A PWM duty ratio generated in a microprocessor is used to indirectly construct the inductor voltage based on the input voltage and the DC-link voltage. The measured inductor current and indirectly constructed inductor voltage are the inputs to a band-pass filter to extract only high-frequency (at the switching frequency, f_{SF}) component as:

$$\frac{\frac{k_1 \cdot 2\pi f_{SF} \cdot S}{Q}}{S^2 + \frac{2\pi f_{SF}}{Q} + (2\pi f_{SF})^2} \tag{1}$$

Where, f_{SF} is the switching frequency and Q is the Q-factor, which is the reciprocal of the fractional bandwidth. The bandpass filter outputs are α-axis inductor voltage ($V^{\alpha}_{L1\_SF}$) and α-axis inductor current ($i^{\alpha}_{L1\_SF}$). After the band-pass filter, the high-frequency inductor current ($i^{\alpha}_{L1\_SF}$) and voltage ($V^{\alpha}_{L1\_SF}$) are applied to an all-pass filter (virtual β axis creation block) to introduce a 90-degree angle shift for an artificially created β-axis component as (2).

$$-\frac{S - 2\pi f_{SF}}{S + 2\pi f_{SF}} \tag{2}$$

Then, the α-β axes signals include only the high-frequency component at the switching frequency, and hence they decrease to zero once a switch fault occurs. The next step is to create easy-to-detect signals using the α-β to d-q transformation based on the position θ_{SF} created by the integral of the switching frequency (f_{SF}).

$$\theta_{SF} = \int 2\pi \cdot f_{SF} \cdot dt \tag{3}$$

Then, the magnitudes of the high-frequency voltage and current using the d-q components can produce the inductor's virtual admittance (Y_{L1_SF}) as

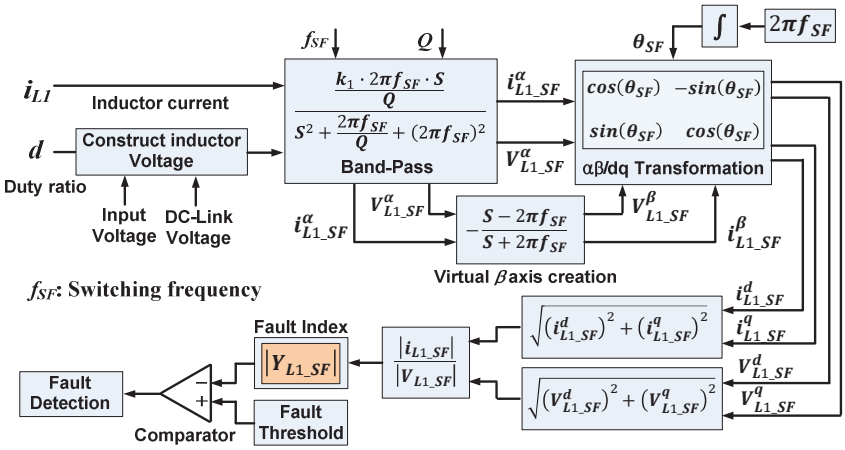

Fig. 2. Switch fault detection procedure based on a high-frequency inductor admittance observation for fuel cell and solar PV converters.

$$\left|Y_{L1\_SF}\right| = \frac{\left|i_{L1\_SF}\right|}{\left|V_{L1\_SF}\right|} = \frac{\sqrt{\left(i^{d}_{L1\_SF}\right)^2 + \left(i^{q}_{L1\_SF}\right)^2}}{\sqrt{\left(V^{d}_{L1\_SF}\right)^2 + \left(V^{q}_{L1\_SF}\right)^2}} \quad (4)$$

Table I presents the dc-dc converter parameters used for simulations and experiments. Fig. 3(a) presents the steady-state response of $i^{\alpha}_{L1\_SF}$ and $i^{\beta}_{L1\_SF}$ waveforms after the bandpass and all-pass filters. For the simulation, a 20 kHz switching frequency has been used, and the bandpass filter's center frequency is the same as the switching frequency. Ideally, as shown in the simulation waveforms, sinusoidal α-β axis currents are observed. The bottom waveform of Fig. 3(a) is the d-q axes' inductor currents after the α-β to d-q transformation at a steady state.

TABLE I
PARAMETERS OF THE NON-ISOLATED DC-DC CONVERTER

Parameters	Value
DC-link Capacitance (C_A, C_B)	470 µF
Input Nominal Voltage	14.8 V
Inductor Size	1 mH
Tested Switching Frequency	5 kHz and 20 kHz

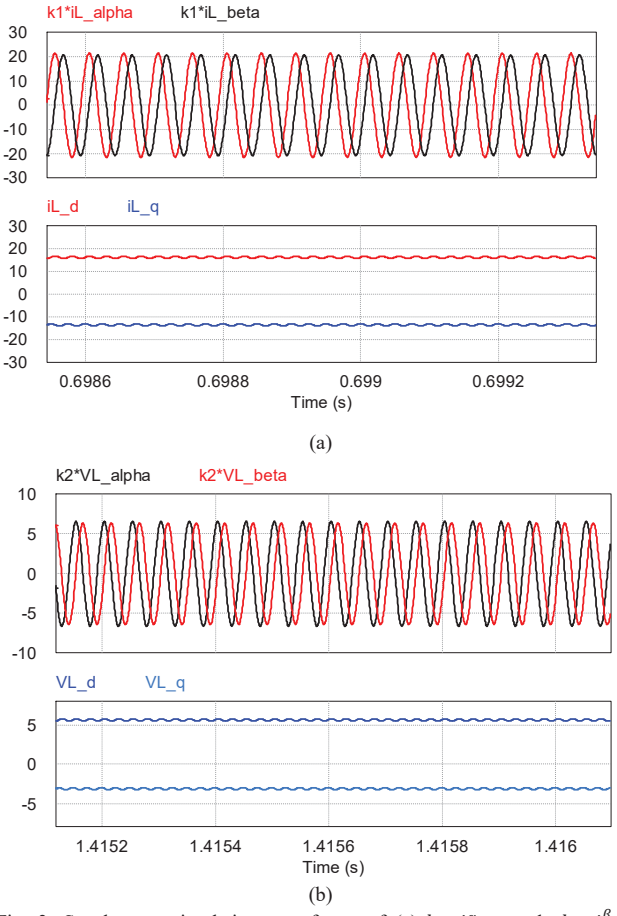

Fig. 3. Steady-state simulation waveforms of (a) $k_1 \cdot i^{\alpha}_{L1\_SF}$ and $k_1 \cdot i^{\beta}_{L1\_SF}$ (upper) and $i^{d}_{L1\_SF}$ and $i^{q}_{L1\_SF}$ (bottom); (b) $k_2 \cdot V^{\alpha}_{L1\_SF}$ and $k_2 \cdot V^{\beta}_{L1\_SF}$ (upper) and $V^{d}_{L1\_SF}$ and $V^{q}_{L1\_SF}$ (bottom). * k1 and k2: constant coefficients.

Fig. 3(b) depicts the steady-state inductor voltage waveforms. As shown in the upper waveform of Fig. 3(b), $V^{\alpha}_{L1\_SF}$ and $V^{\beta}_{L1\_SF}$ have 90° angle shift with a sinusoidal shape. In addition, the bottom waveform presents the d-q axes inductor voltage waveforms ($V^{d}_{L1\_SF}$ and $V^{q}_{L1\_SF}$). For the simulation study, a 20 kHz switching frequency has been selected to test the proposed fault detection strategy. For the detection performance observation under load changes, an additional simulation study has been done.

As shown in Fig. 4, an extreme load change was created on purpose at 0.8 sec to observe the influence on the inductor admittance amplitude at the switching frequency ($\left|Y_{L1\_SF}\right|$). The load change is from a heavier load to a lighter load, and hence the output capacitor voltage (V_{CB1}) has been suddenly increased after 0.8 sec, as shown in Fig. 4 (a). The sudden load change at 0.8 sec creates significant perturbations on inductor currents, inductor voltages, and capacitor voltage. However, the fault index waveform (in Fig. 4(b)), which is created by the virtual inductor admittance (at the switching frequency), is less sensitive to the load variation created at 0.8 second since the load change influences both numerator and denominator of eq (4).

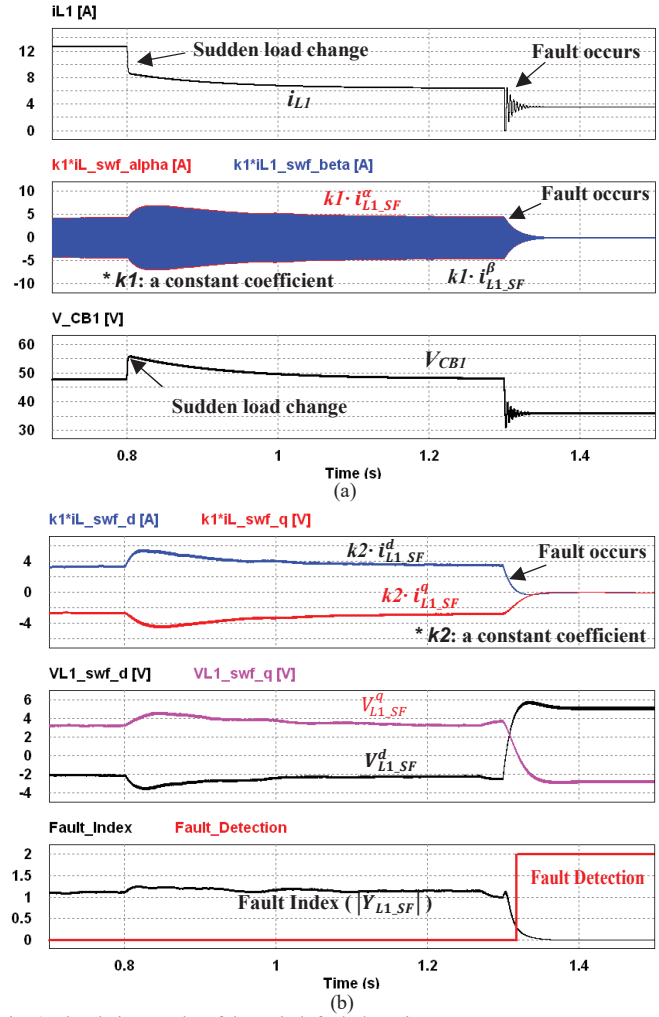

Fig. 4. Simulation results of the switch fault detection.

After an open switch fault created at 1.3 sec, the fault index signal based on the virtual inductor admittance decreases to zero and a fault signal is triggered since the fault index is lower than a pre-determined threshold value. It should be noted that the fault index function can reduce false alarm occurrences significantly during sudden load changes since it is less sensitive to highly dynamic load variations.

To verify the feasibility of the proposed fault detection method, an experimental study has been performed using the Texas Instruments F28004x DSP as the main controller. For the experimental test, a 5 kHz switching frequency has been used, and the bandpass filter's center frequency was set to 5 kHz as well.

Fig. 5 presents dc-link capacitor voltage, inductor current, and α-β inductor currents under a sudden load change (lighter to heavier load change). The α-β axis current components are created based on the bandpass filtering at the switching frequency (α axis) and all-pass filtering (virtual β axis), and they have a 90° angle shift. As observed in the waveform, the sudden load change generates significant perturbations on inductor voltages and currents, and hence a fault index function (based on the virtual admittance) that can reduce the influence is required to avoid false alarms. In Fig. 6, the system response under two load changes and a switch fault is presented. Under load changes, the fault index function shown in Fig. 6(b) (CH 3) can effectively suppress the perturbation even though other parameters go through larger perturbations. This can minimize the false alarms due to load and flight condition changes that occur frequently during a flight mission of UAVs.

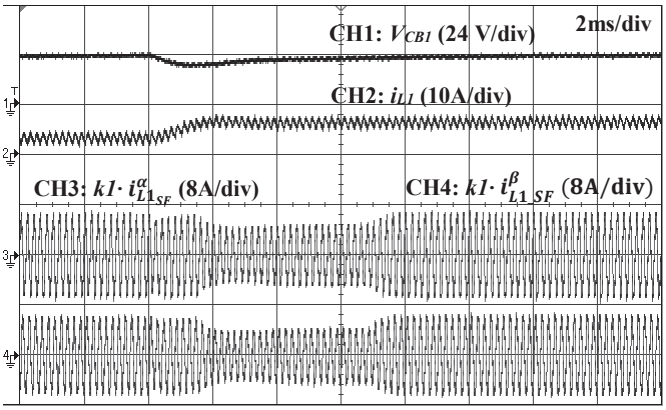

Fig. 5. Experimental waveforms under a sudden load change (CH1: dc-link voltage, V_{CB1}; CH2: inductor current, i_{L1}; CH3: $k1\cdot i^{\alpha}_{L1_{SF}}$; CH4: $k1\cdot i^{\beta}_{L1\_SF}$). * $k1$: a constant coefficient.

The amplitude of α-β components at the switching frequency decreases after a switch fault occurrence (OSF is exemplified), as shown in Fig. 6. As aforementioned, the high-frequency inductor admittance at the switching frequency is less sensitive to load changes due to a cancellation effect by the division in eq (4) because the load changes are reflected in both the inductor current (numerator) and inductor voltage (denominator).

The two load changes (lighter to heavier and heavier to lighter) were created on purpose to monitor the influence on the virtual admittance ($|Y_{L1\_SF}|$) that is used as a fault index function.

After an open switch fault, the fault index based on the virtual inductor admittance decreases to zero, and a fault detection signal is triggered since the fault index is lower than a pre-determined threshold value. Fig. 6(b) presents the fault index function (CH3) and fault detection signal (CH4). The experimental results verify the feasibility of the detection technique based on the virtual admittance signal formulated at the switching frequency under α-β and d-q transformations to reduce the influence of load and flight condition changes in UAVs. It is expected that this new detection approach can improve accuracy without additional coils or sensors and have reasonable software complexity.

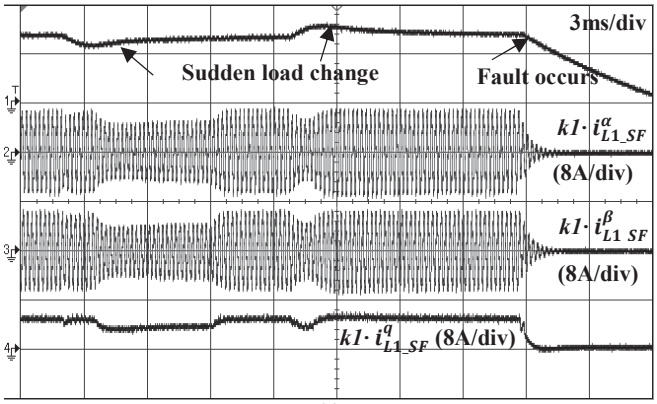

(a)

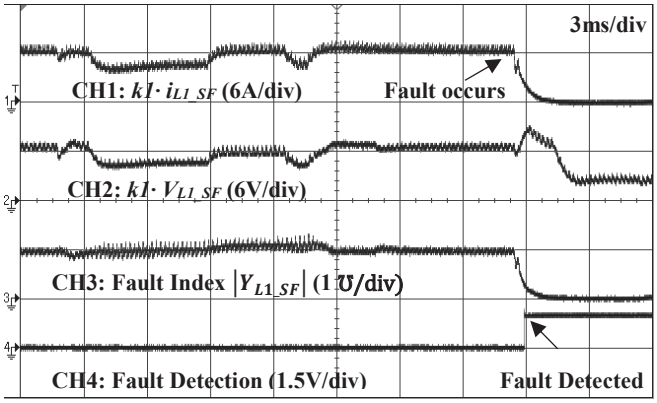

(b)

Fig. 6. Experimental waveforms under sudden load changes and a switch fault. * $k1$: a constant coefficient.

III. Conclusions

In this paper, a novel switch fault detection technique for hybrid UAVs has been investigated to enhance the sensitivity of fault identification, which can eventually improve the reliability of the UAVs. The inductor currents and voltages at a switching frequency were derived first based on a bandpass filter. Then, α-β and d-q transformations were applied to extract a fault signature that is less sensitive to load variations.

A virtual admittance-based fault index function was eventually developed to improve the accuracy of fault detection, especially for the UAV application, which suffers significant load changes. The proposed concept and the switch fault detection technique were discussed, and their feasibility was verified by simulation and experimental studies. It is expected that the detection method can also be applied to various other application areas with dc-dc converters.

ACKNOWLEDGMENT

This work was supported by an NSF (National Science Foundation) grant under award no. 2321681, including an REU supplement.

REFERENCES

[1] B. Lee, S. Kwon, P. Park and K. Kim, "Active power management system for an unmanned aerial vehicle powered by solar cells, a fuel cell, and batteries," in IEEE Transactions on Aerospace and Electronic Systems, vol. 50, no. 4, pp. 3167-3177, October 2014.

[2] M. N. Boukoberine, Z. Zhou and M. Benbouzid, "Power Supply Architectures for Drones - A Review," IECON 2019 - 45th Annual Conference of the IEEE Industrial Electronics Society, Lisbon, Portugal, 2019, pp. 5826-5831.

[3] A. Gong, R. MacNeill, D. Verstraete and J. L. Palmer, "Analysis of a Fuel-Cell/Battery/Supercapacitor Hybrid Propulsion System for a UAV using a Hardware-in-the-Loop Flight Simulator," 2018 AIAA/IEEE Electric Aircraft Technologies Symposium, Cincinnati, Ohio, 2018.

[4] S. Dusmez, H. Duran and B. Akin, "Remaining Useful Lifetime Estimation for Thermally Stressed Power MOSFETs Based on on-State Resistance Variation," in IEEE Transactions on Industry Applications, vol. 52, no. 3, pp. 2554-2563, May-June 2016.

[5] S. Nie, X. Pei, Y. Chen and Y. Kang, "Fault diagnosis of PWM DC–DC converters based on magnetic component voltages equation", IEEE Trans. Power Electron., vol. 29, no. 9, pp. 4978-4988, Sep. 2014.

[6] M. Shahbazi, E. Jamshidpour, P. Poure, S. Saadate and M. Zolghadri, "Open and short-circuit switch fault diagnosis for non-isolated DC-DC converters using field programmable gate array", IEEE Trans. Ind. Electron., vol. 60, no. 9, pp. 4136-4146, Sep. 2013.

[7] E. Jamshidpour, P. Poure, E. Gholipour and S. Saadate, "Single-switch DC–DC converter with fault-tolerant capability under open- and short-circuit switch failures", IEEE Trans. Power Electron., vol. 30, no. 5, pp. 2703-2712, May 2015.

[8] E. Farjah, H. Givi and T. Ghanbari, "Application of an efficient rogowski coil sensor for switch fault diagnosis and capacitor ESR monitoring in non-isolated single switch DC-DC converters", IEEE Trans. Power Electron., vol. 32, no. 2, pp. 1442-1456, Feb. 2017.

[9] E. Jamshidpour, P. Poure and S. Saadate, "Photovoltaic systems reliability improvement by real-time FPGA-based switch failure diagnosis and fault-tolerant DC-DC converter", IEEE Trans. Ind. Electron., vol. 62, no. 11, pp. 7247-7255, Nov. 2015.

[10] E. Ribeiro, A. J. M. Cardoso and C. Boccaletti, "Open-circuit fault diagnosis in interleaved DC–DC converters", IEEE Trans. Power Electron., vol. 29, no. 6, pp. 3091-3102, Jun. 2014.

[11] H. Givi, E. Farjah and T. Ghanbari, "Switch fault diagnosis and capacitor lifetime monitoring technique for DC–DC converters using a single sensor", IET Sci. Meas. Technol., vol. 10, no. 5, pp. 513-527, Aug. 2016.

[12] Y. Chen, X. Pei, S. Nie and Y. Kang, "Monitoring and diagnosis for the DC–DC converter using the magnetic near field waveform", IEEE Trans. Ind. Electron., vol. 58, no. 5, pp. 1634-1647, May 2011.

[13] B. Lu and S. K. Sharma, "A literature review of IGBT fault diagnostic and protection methods for power inverters", IEEE Trans. Ind. Appl., vol. 45, no. 5, pp. 1770-1777, Sep./Oct. 2009.

[14] H. Givi, E. Farjah and T. Ghanbari, "Switch and diode fault diagnosis in non-isolated DC-DC converters using diode voltage signature", IEEE Trans. Ind. Electron., vol. 65, no. 2, pp. 1606-1615, Feb. 2018.

[15] T. Kim, H. Lee and S. Kwak, "Open-Circuit Switch-Fault Tolerant Control of a Modified Boost DC–DC Converter for Alternative Energy Systems," IEEE Access, vol. 7, pp. 69535-69544, 2019.

[16] E. Ribeiro, A. J. M. Cardoso and C. Boccaletti, "Fault-tolerant strategy for a photovoltaic DC-DC converter", IEEE Trans. Power Electron., vol. 28, no. 6, pp. 3008-3018, Jun. 2013.